

A frequency-domain perspective on GW150914 ringdown overtone

Yi-Fan Wang (王一帆),^{1,2,3,*} Collin D. Capano,^{4,2,3} Jahed Abedi,^{5,2,3} Shilpa Kastha,^{6,2,3}
Badri Krishnan,^{7,2,3} Alex B. Nielsen,⁵ Alexander H. Nitz,⁸ and Julian Westerweck^{2,3,9}

¹Max-Planck-Institut für Gravitationsphysik (Albert-Einstein-Institut), Am Mühlenberg 1, D-14476 Potsdam, Germany

²Max-Planck-Institut für Gravitationsphysik (Albert-Einstein-Institut), Callinstraße 38, D-30167 Hannover, Germany

³Leibniz Universität Hannover, D-30167 Hannover, Germany

⁴Department of Physics, University of Massachusetts, Dartmouth, MA 02747, USA

⁵Department of Mathematics and Physics, University of Stavanger, NO-4036 Stavanger, Norway

⁶Niels Bohr International Academy, Niels Bohr Institute, Blegdamsvej 17, 2100 Copenhagen, Denmark

⁷Institute for Mathematics, Astrophysics and Particle Physics,

Radboud University, Heyendaalseweg 135, 6525 AJ Nijmegen, The Netherlands

⁸Department of Physics, Syracuse University, Syracuse, NY 13244, USA

⁹Institute for Gravitational Wave Astronomy and School of Physics and Astronomy,
University of Birmingham, Edgbaston, Birmingham B15 2TT, United Kingdom

We revisit the recent debate on the evidence for an overtone in the black hole ringdown of GW150914. By gating and inpainting the data, we discard the contamination from earlier parts of the gravitational wave signal before ringdown. This enables the parameter estimation to be conducted in the frequency domain, which is mathematically equivalent to the time domain method. We keep the settings as similar as possible to the previous studies by Cotesta *et al.* [1] and Isi *et al.* [2, 3] which yielded conflicting results on the Bayes factor of the overtone. We examine the spectral contents of the matched-filtering in the frequency domain, and propose a convergence test to assess the validity of an overtone model. Our results find the Bayes factors for the overtone fall within 10 and 26 around a range of times centered at the best-fit merger time of GW150914, which supports the existence of an overtone in agreement with the conclusions of Isi *et al.* [2, 3]. Our work contributes to the understanding of how various methods affect the statistical significance of overtones.

I. INTRODUCTION

The gravitational waves (GWs) emitted during the black hole (BH) ringdown consists of a superposition of damped sinusoids known as quasi-normal modes (QNMs) [4]. According to the no-hair theorem [5, 6] the characteristic frequencies and damping times are exclusively determined by the astrophysical BH's mass and spin. When multiple modes are identified from the ringdown's GW, the BH mass and spin can be inferred independently and cross-checked. This is often known as BH spectroscopy [7], and offers an unequivocal way to test the validity of general relativity (GR).

The first evidence of a QNM is reported for GW150914 [8], in which the single $(\ell, m, n) = (2, 2, 0)$ mode is found with a frequency and decay time consistent with the GR expectation from the full signal analysis. Theoretical studies [9] suggest the detection of a secondary QNM would likely only occur once Advanced LIGO [10], Advanced Virgo [11] and KAGRA [12] have reached their design sensitivity. Nevertheless, the event GW190521 is discovered to have an unexpectedly high redshifted remnant mass $\sim 260 M_{\odot}$ [13, 14]. The evidence of a subdominant mode $(3, 3, 0)$ from GW190521 is reported with a Bayes factor of 56 [15–18]; also see [19] for an alternative interpretation involving the $(2, 1, 0)$ mode. By fitting numerical relativity data, Ref. [20] shows that the

QNM description can be valid as early as the merger stage, provided that overtones are considered. Starting the analysis from the merger time, Isi *et al.* [2] reports the first detection of a $(2, 2, 1)$ mode from GW150914 with a significance of 3.6σ and shows the parameters to be consistent with the prediction of GR. More studies that investigate the GW150914 overtone include [21–24] with various techniques.

However, Cotesta *et al.* [1] claims that the detection of the overtone in Isi *et al.* [2] is noise-dominated. A reanalysis shows that the Bayes factor in favor of the overtone compared to only the fundamental mode is less than 1 around the merger time, hence no evidence for the overtone is found. Nevertheless, Isi and Farr [3] revisits the analysis and claims to be unable to reproduce the results in Cotesta *et al.* [1] and shows that the Bayes factor of the model including the $(2, 2, 1)$ mode indicates the presence of the overtone.

The data analysis frameworks employed in [1] and [2, 3] are fundamentally similar. To remove the influence of the pre-ringdown GW signal, both compute the likelihood in the time domain [25, 26], as the frequency-domain formalism used by conventional GW parameter estimation is no longer applicable. In practice, a number of technical complications can result in the inconsistent findings between [1] and [2, 3], highlighting the need for a comprehensive understanding of the techniques employed in ringdown overtone analysis. In this study, we utilize an independent framework in the frequency domain to revisit GW150914, aiming to offer a new perspective to understand the analysis for overtones.

* yifan.wang@aei.mpg.de

In [15] we propose a new approach following the original idea of [27] to excise the contamination from the GW signal prior to the ringdown by gating and inpainting the data. This is mathematically equivalent to the time domain method of [1–3] and enables us to keep the analysis in the frequency domain. Thereby, we can take advantage of the parameter estimation package `PyCBC inference` [28] by using several existing modules, such as data conditioning, power spectral density (PSD) estimation with Welch’s method [29], and frequency-domain likelihood calculation and sampling [30], which are well tested and were used in numerous previous studies, e.g., [31, 32].

We explore the impact of different sampling rates on the GW150914 overtone significance as the sampling rate appears to differ between [1] and [2, 3] (16384 Hz vs 2048 Hz). In addition, the extremely short decay time of the overtone, typically $\lesssim \mathcal{O}(1)$ ms, motivates us to examine the matched-filtering of high frequency contents of the signal, which is straightforward by examining the waveform in the frequency domain. As emphasized by [1], the merger time of GW150914 is subject to uncertainty, and we follow [1–3] to select a set of discrete times centered around the best-fit merger time as the ringdown starting time.¹ We also carefully ensure the starting time is precisely implemented in `PyCBC inference`, rather than rounding up to that of a LIGO data sample, in light of our findings that the evidence of an overtone is highly sensitive to such approximations (see Appendix A) because of the overtone’s rapid decay.

II. GATED GAUSSIAN LIKELIHOOD

We briefly review the gated Gaussian likelihood that employs data gating and inpainting [15, 26, 27]. The conventional likelihood used in GW parameter estimation for Gaussian and stationary noise is

$$\mathcal{L}(\mathbf{n}) = \frac{1}{\sqrt{(2\pi)^N |C|}} \exp \left[-\frac{1}{2} \mathbf{n}^T C^{-1} \mathbf{n} \right] \quad (1)$$

where \mathbf{n} is the noise vector with N elements, C is the covariance matrix of \mathbf{n} . By the stationary assumption, C is a Toeplitz matrix, and can be further diagonalized by a discrete Fourier transform basis matrix if the noise data is circulant. Therefore, the likelihood can be greatly simplified in the frequency domain as

$$\ln \mathcal{L}(\mathbf{n}) \propto \langle \mathbf{n} | \mathbf{n} \rangle \quad (2)$$

where the inner product is defined as

$$\langle a | b \rangle = 4\Re \int \frac{\tilde{a}^\dagger(f) \tilde{b}(f)}{S_n(f)} df \quad (3)$$

¹ See [33] which reports the analysis for GW150914 overtone by sampling and marginalizing over the sky location and starting time.

in which $\tilde{a}(f)$ and $\tilde{b}(f)$ are the Fourier transforms of arbitrary functions a and b , and $S_n(f)$ is the one-sided PSD of the noise. When a GW is present, the noise can be obtained by subtracting the GW waveform \mathbf{h} from the detector measurement \mathbf{d} , so that the likelihood of a GW waveform is $\mathcal{L}(\mathbf{n}) = \mathcal{L}(\mathbf{d} - \mathbf{h})$.

Ringdown inference aims to exclusively analyze signals after the remnant BH enters a linear perturbation regime, hence the pre-ringdown contamination should be excised. However, this would break the circularity condition due to the abrupt onset of the ringdown signal, thus the covariance matrix can not be diagonalized simply by a Fourier transform [26]. One needs to numerically invert the non-circulant covariance matrix in Eq. (1), as implemented by the time domain analysis [1–3].

Alternatively, Ref. [27] proposes, and Ref. [15] applies in ringdown analysis, a relation between the inversion of the covariance matrix from truncated data, \mathbf{n}_{tr} , and that from the complete data, \mathbf{n} , by replacing (inpainting) the excised data with \mathbf{x} . Without loss of generality, we express the complete data \mathbf{n} as the concatenation of three vectors, which is $\mathbf{n} = \mathbf{n}_1 \oplus \mathbf{n}_2 \oplus \mathbf{n}_3$, where \oplus denotes the concatenation operation; the border of \mathbf{n}_2 and \mathbf{n}_3 delineates the pre-ringdown and ringdown stage, and \mathbf{n}_2 is long enough to cover the entire pre-ringdown GW signals. The truncated data can be expressed by $\mathbf{n}_{\text{tr}} = \mathbf{n}_1 \oplus \mathbf{n}_3$. The gated Gaussian likelihood aims to replace \mathbf{n}_2 with a vector \mathbf{x} , as $\mathbf{n}_{\text{inpainted}} = \mathbf{n}_1 \oplus \mathbf{x} \oplus \mathbf{n}_3$, such that

$$\mathbf{n}_{\text{tr}} C_{\text{tr}}^{-1} \mathbf{n}_{\text{tr}} = \mathbf{n}_{\text{inpainted}}^T C^{-1} \mathbf{n}_{\text{inpainted}} \quad (4)$$

where C_{tr}^{-1} denotes the covariance matrix of \mathbf{n}_{tr} . The solution is obtained by solving the Toeplitz linear equation (for a proof see Appendix C)

$$[C^{-1}(\mathbf{n}_1 \oplus \mathbf{x} \oplus \mathbf{n}_3)]_{\text{inpainted}} = \mathbf{0}_{\text{inpainted}} \quad (5)$$

where the subscript asserts this equation is valid only in the rows corresponding to the data being inpainted. Given an M -dimensional inpainting vector \mathbf{x} , Eq. (5) is an M -dimensional Toeplitz linear equation with the time complexity scaling as M^2 . Since the right-hand side of Eq. (4) resumes the use of C^{-1} , one can diagonalize it with a Fourier transform and thus perform the analysis in the frequency domain once \mathbf{x} is obtained via Eq. (5).

III. RESULTS

We reanalyze the overtone of GW150914 using similar settings to [1–3]. Our waveform model is

$$h_+ + ih_\times = \sum_{\ell mn} {}_{-2}S_{\ell mn}(\iota, \varphi; \chi_f) A_{\ell mn} e^{i(\Omega_{\ell mn} t + \phi_{\ell mn})}, \quad (6)$$

where ${}_{-2}S_{\ell mn}$ are the spin-weighted spheroidal harmonics, ι and φ are the inclination angle and azimuthal angle; $\Omega_{\ell mn} = 2\pi f_{\ell mn} + i/\tau_{\ell mn}$ is the complex frequency, $f_{\ell mn}$ and $\tau_{\ell mn}$ are the characteristic frequency and decay time

exclusively determined by M_f and χ_f , the mass and spin of the remnant BH; $A_{\ell mn}$ and $\phi_{\ell mn}$ are the amplitude and initial phase, which in principle can be determined by the initial conditions of the BH perturbation, however, due to lack of concrete knowledge, we treat them as free parameters to be inferred from the data.

We follow [1] and use the reference GPS time $t_{\text{ref}} = 1126259462.42323$ s as a median of GW150914’s merger time recorded by LIGO Hanford, and expand the analysis by scanning different starting times within $t_{\text{ref}} \pm 1.5$ ms, corresponding to 2σ uncertainty around t_{ref} . The amplitude priors on A_{220} and A_{221} are uniform in $[0, 5 \times 10^{-20}]$; the phase priors on ϕ_{220} and ϕ_{221} are uniform in $[0, 2\pi]$; all of which are identical to [1]. The prior of final mass and final dimensionless spin is chosen to be uniform in $[35, 140] M_{\odot}$ and $[0, 0.99]$; the inclination angle, azimuthal angle, polarization angle and sky localization are fixed to the values given by [1–3], which in turn are obtained from the maximum likelihood value from the analysis of the complete signal of GW150914. Because the auto correlation function (ACF) of LIGO data typically decays to zero only after a few seconds [26], we analyze 8 s of data centered at the starting time. We also use four different sampling rates f_s from 1024 Hz to 8192 Hz to study the impact of different upper frequency limits on the overtone inference. No higher sampling rate is considered because the LIGO data calibration is only valid from 10 Hz to 5 kHz [34].

The findings of our study are presented in Fig. 1, which shows the logarithm of the Bayes factor $\log_{10} \mathcal{B}_{220}^{221}$ comparing the waveform model with modes $(2, 2, 0) + (2, 2, 1)$ to that with only the $(2, 2, 0)$ mode at various starting times. For comparison, we plot the Bayes factors reported by [1] and [3], respectively. We consider the $f_s = 8192$ Hz runs as our fiducial results and quantify the convergence of Bayes factors by measuring the fractional difference between the highest and second highest sampling rate results, i.e., $\delta = |\mathcal{B}_{f_s=8192} - \mathcal{B}_{f_s=4096}| / \mathcal{B}_{f_s=8192}$, as shown in Fig. 1.

We notice the intriguing trend that the Bayes factors from different sampling rates only start to converge after $t_{\text{ref}} - 0.25$ ms, where we quantify convergence by the criterion $\delta < 50\%$. Prior to that, there are noticeable disagreements from different sampling rates. Results with $f_s = 1024$ Hz yield the strongest evidence for the $(2, 2, 1)$ mode (we will discuss in more details in the next section). We regard the divergence as an indicator that the overtone model is matching the data insufficiently. The strong Bayes evidence for low sampling rate can be plausibly attributed to matching the pre-ringdown stage of GW150914 which has a merger frequency ~ 175 Hz [35, 36]. Extending the high-frequency cutoff towards greater values would result in increasing inconsistencies between the template and the signal. In light of this observation, we propose a discriminator that utilizes the (non-)convergence of results from various sampling rates to determine the region where the ringdown overtone model is applicable, as opposed to the region where pre-

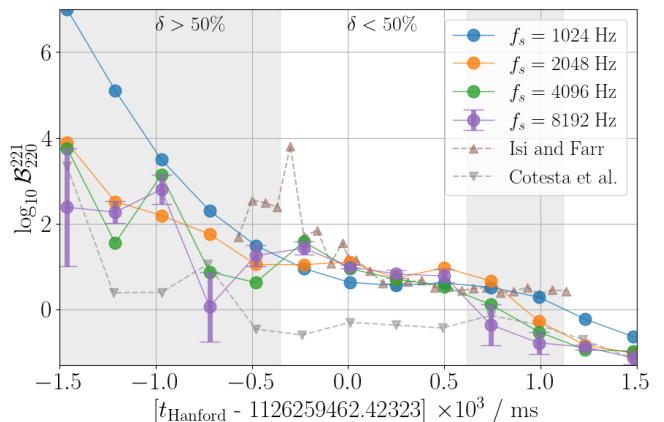


FIG. 1. The logarithm of Bayes factors comparing the $(2, 2, 0) + (2, 2, 1)$ model and the $(2, 2, 0)$ -only model with respect to a variety of starting times for sampling rates $f_s = 1024/2048/4096/8192$ Hz. As a comparison, we plot the Bayes factors obtained from [1, 3]. We also plot symmetric error bars with length $\mathcal{B}_{f_s=8192} \times \delta$. The shaded regions depict where the results from different sampling rates have not converged, quantified by $\delta > 50\%$, while in the non-shaded region all have $\delta < 50\%$.

ringdown contamination is present. Signal consistency tests in a similar spirit have been proposed, e.g., for searching for GWs [37]. At the late time around $t_{\text{ref}} + 1$ ms, we again observed discrepancies of different sampling rates, suggesting the overtone model is again not applicable.

Around the best-fit merger time of GW150914, specifically in $[-0.25, 0.5]$ ms, we obtain converged Bayes factors from four different sampling rates consistently greater than 1 in favor of the existence of the $(2, 2, 1)$ mode. In particular, at $t_{\text{ref}} - 0.25$ ms, which was considered as the merger time by Isi *et al.* [2], we find $\mathcal{B}_{220}^{221} = 26$, the median of A_{221} deviates from zero with 2.8σ ; at t_{ref} , we find $\mathcal{B}_{220}^{221} = 10$, and a 2.5σ non-zero A_{221} , which indicates positive but moderate evidence for the presence of the $(2, 2, 1)$ mode.

Notably, our Bayes factors agree with those from Isi and Farr [3] in and only in the convergence region $[-0.25, 0.5]$ ms. Nevertheless, there is a discrepancy at -0.3 ms with a notable outlier identified to have $\log_{10} \mathcal{B} \sim 4$ by [3]. Given their finer time stride, we further perform additional analyses with $f_s = 2048$ Hz with more finely spaced starting times, but can not reproduce the significant Bayes factor. After $t_{\text{ref}} + 0.75$ ms, our results coincide with Cotesta *et al.* [1], indicating no overtone is found at a late time. To understand how various methods affect the statistical significance of the overtone, we note that a primary difference is that [2, 3] and [1] use a 0.2 s and 0.1 s duration for data analysis, respectively, while we use 8 s to account for the non-zero ACF over a few seconds; thus we conclude a sufficiently long analysis duration can enhance the statistical significance of finding an overtone.

IV. UNDERSTANDING THE DISCREPANCY FROM DIFFERENT SAMPLING RATES

Prior to $t_{\text{ref}} - 0.25$ ms, we notice a divergence of results from four different sampling rates. To better understand its origin, we choose a particular time $t_{\text{ref}} - 0.75$ ms, which shows discrepancies, and analyze the results of parameter estimation in depth. In Fig. 2, we consider the waveforms h_f^{maxL} from parameters corresponding to the maximum likelihood sample. We plot $2|h_f^{\text{maxL}}|\sqrt{f}$ such that the area under the square ratio between the waveform and the amplitude spectral density (ASD) indicates the signal-to-noise ratio (SNR).

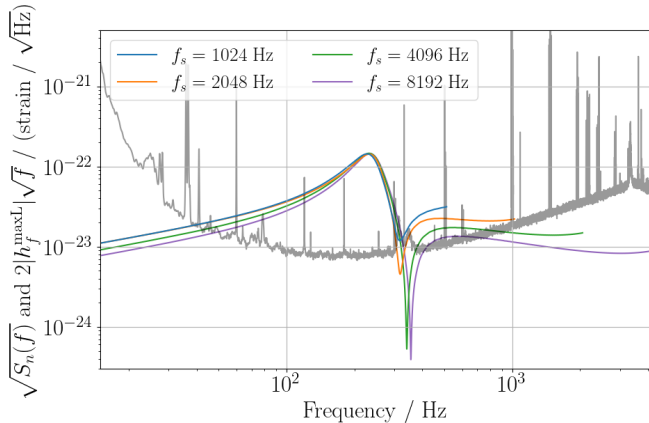


FIG. 2. The maximum likelihood parameters' waveform for four different sampling rates with analysis starting time $t_{\text{ref}} - 0.75$ ms. The grey curve shows the amplitude spectral density $\sqrt{S_n(f)}$.

We notice that the $f_s = 1024$ Hz result tends to favor a waveform with higher amplitude at the Nyquist frequency 512 Hz. Examining the overtone amplitude A_{221} reveals that a stronger (2, 2, 1) mode is favored, which manifests as the tilt at high frequency due to the short decay time (~ 1.5 ms) of the overtone. The rapid decay leads to a broader frequency-domain representation of the waveform. However, when the data analysis is extended to higher frequency bands, this strong (2,2,1) mode is no longer preferred. The SNR also gradually decays from 13.75 to 13.7, 13.3, and 13 for sampling rates increasing from 1024 Hz to 8192 Hz. The discrepancies suggest the starting time is too early and overtone templates do not match the data well. The low sampling rate result tends to be more affected by the contamination from the pre-ringdown to produce a high SNR.

To further illustrate this with the entire posterior instead of a single point from maximum likelihood, we plot the mass and spin posterior distribution in Fig. 3. For all (M_f, χ_f) , we also compute the characteristic decay time of the overtone, τ_{221} , predicted from GR as the background of the figure. Fig. 3 shows that the 8192 Hz result extends to a region with a longer decay time, while the low sampling rate results are more restricted to a shorter

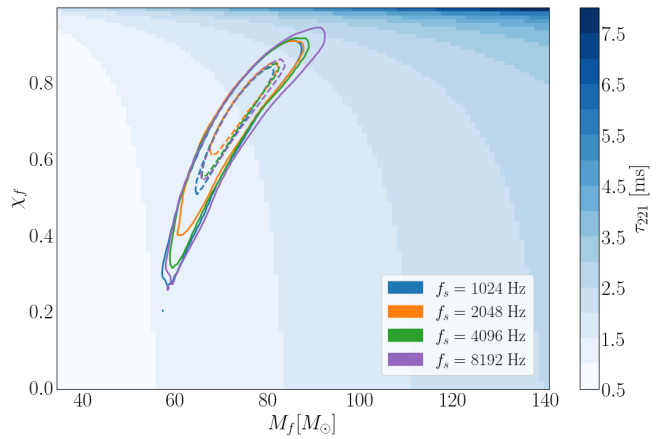


FIG. 3. The marginal posterior of M_f and χ_f for four different sampling rates with analysis starting time $t_{\text{ref}} - 0.75$ ms. In the background, we plot the value of τ_{221} as expected in GR as a function of the mass and spin of a Kerr BH. The solid and dashed lines show the 90% and 50% credible regions, respectively.

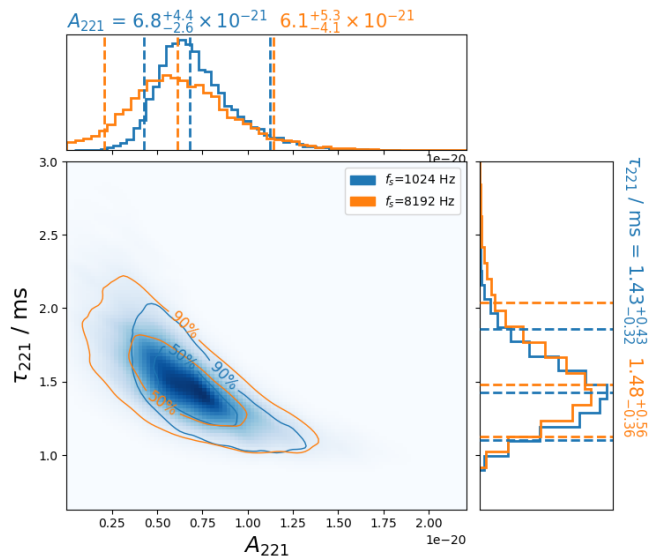


FIG. 4. A comparison of the posteriors for A_{221} and τ_{221} using two different sampling rates, 1024 Hz and 8192 Hz, with analysis starting time $t_{\text{ref}} - 0.75$ ms. The contours denote the 90% and 50% credible regions. The shaded region shows the posterior probability density of the $f_s = 1024$ Hz result.

decay time. The posterior of τ_{221} and A_{221} is plotted in Fig. 4, showing the parameters' negative correlation. The 8192 Hz result favors a longer decay time τ_{221} , hence a higher posterior density at $A_{221} = 0$. Using the Savage-Dickey density ratio, the density of $A_{221} = 0$ directly determines \mathcal{B}_{220}^{221} . We thus conclude that the (dis-) favoring of shorter τ_{221} , which in turn is directly related to the signal intensity in high-frequency bands, by an inappropriate sampling rate can bias the posterior of A_{221} , and

thus enhance or weaken the evidence for a $(2, 2, 1)$ mode. The findings underscore the importance of examining the frequency spectrum in order to determine an appropriate time range within which a ringdown overtone model is applicable.

V. CONCLUSION AND DISCUSSION

We revisit the GW150914 overtone using an independent frequency-domain analysis, with settings as similar as possible to [1–3]; notably we use an 8s data analysis duration accounting for the non-zero ACF. We examine the frequency spectral content of the recovered waveforms and interpret the divergence of results from different sampling rates as evidence for where the overtone model is not valid to be matched with the data. When the results converge around the merger time of GW150914, we find Bayes factor values fall within the range of 10 to 26, which supports the existence of an overtone, in agreement with the conclusion of [2, 3]. We show that starting the analysis too early or too late will lead to discrepancies for different sampling rates. At too early times, an inappropriately low sampling rate tends to favor a signal with a shorter decay time and thus biases the estimation towards stronger evidence for the $(2, 2, 1)$ mode. In light of these discoveries, we propose a new strategy, from the data analysis perspective, by analyzing the convergence of different sampling rates to determine the validity of the overtone model, complementary to the efforts of, e.g., [38, 39], which address whether the overtone is valid physically.

Recently, the authors of Refs. [2, 3] published a comment showing that increasing the analysis duration and correcting the approximation of starting time discretization can alleviate the discrepancies [40]. However, the authors of [1] replied that the logarithmic Bayes factors are still negative after addressing the comments [41]. Our method in the current work does not have any of the aforementioned limitations as we have used a long analysis duration (8s) and reconstructed the subsampling data point to ensure the starting time is precise (Appendix A). Our work shows that using these more robust choices will affect the results in the direction of enhancing the statistical significance of an overtone.

We release the scripts to reproduce this work and the posterior files at [42].

ACKNOWLEDGMENTS

Y.-F.W. acknowledges the Max Planck Gesellschaft, the Atlas computing team, and AEI Hannover where the majority of this work was done; he also thanks Gregorio Carullo, Max Isi and Will Farr for insightful comments. A.H.N. acknowledges support from NSF grant PHY-2309240. S.K. acknowledges support from the Villum Investigator program supported by the VILLUM

Foundation (grant no. VIL37766) and the DNRF Chair program (grant no. DNRF162) by the Danish National Research Foundation. This project has received funding from the European Union’s Horizon 2020 research and innovation programme under the Marie Skłodowska-Curie grant agreement No 101131233. This research has made use of data from the Gravitational Wave Open Science Center (<https://www.gw-openscience.org>), a service of LIGO Laboratory, the LIGO Scientific Collaboration and the Virgo Collaboration. LIGO is funded by the U.S. National Science Foundation. Virgo is funded by the French Centre National de Recherche Scientifique (CNRS), the Italian Istituto Nazionale della Fisica Nucleare (INFN) and the Dutch Nikhef, with contributions by Polish and Hungarian institutes.

Appendix A: Ensuring a precise starting time for ringdown analysis

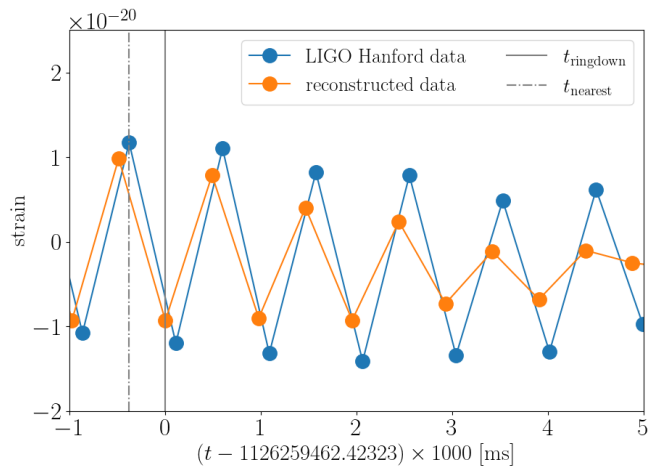


FIG. 5. Reconstructing the subsample corresponding to the starting time of ringdown, t_{ringdown} . This is done by time shifting the data by an offset of the difference of t_{ringdown} and t_{nearest} which corresponds to the nearest data sample from LIGO Hanford.

The gating and inpainting formalism is potentially subject to a subtle caveat that the starting and ending time of the inpainting can only land on a specific data point due to the discrete nature of the sampled data. This issue is particularly severe for a lower sampling rate with a coarser time resolution. As depicted in Fig. 1 in the main text, the results are sensitive to the ringdown starting time at a sub-millisecond level because of the rapid decay of an overtone. Consequently, it is necessary to ensure a precise starting time for the ringdown analysis.

We address this issue by reconstructing the sub-data points from the sampled data at the starting time of the ringdown, t_{ringdown} , which is achieved by time shifting in the frequency domain by an offset between t_{ringdown}

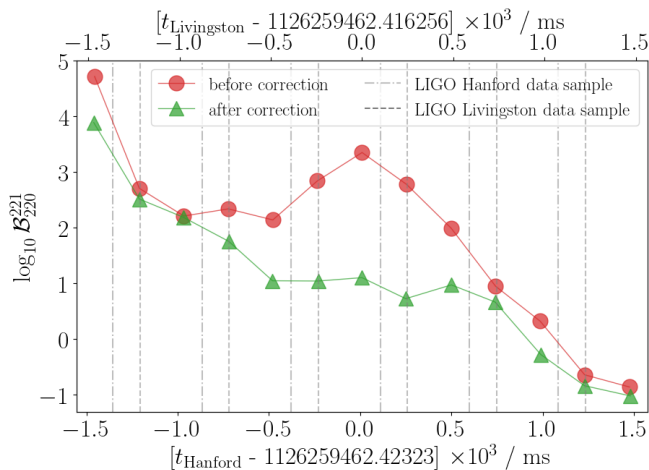


FIG. 6. The results of logarithm Bayes factor from sampling rate 2048 Hz before and after accounting for the issue when the ringdown starting time lands on a subsample. The vertical (dot) dashed lines indicates the time stamp of the data samples from LIGO Hanford or Livingston.

and the time stamp of the floor-nearest data sample, t_{nearest} . To visualize, the discrete data samples from the LIGO Hanford with $f_s = 2048$ Hz and those being re-constructed are plotted in Fig. 5. In Fig. 6 we also plot the results of $\log_{10} \mathcal{B}_{220}^{221}$ from $f_s = 2048$ Hz before and after accounting for this issue. To guide the eyes, we also plot vertical dashed lines for the time stamps for the sampled data of LIGO Hanford and Livingston. Before addressing this problem, the starting time of ringdown, or equivalently, the ending time of inpainting, is rounded up to the floor-nearest time of a data sample. Therefore, this effectively results in an earlier and incoherent starting time between LIGO Hanford and Livingston, biasing the Bayes factors towards higher values due to the contamination from signals prior to ringdown.

Appendix B: Parameterization of the relative amplitude between (2,2,1) and (2,2,0)

We also implement a different parameterization to examine the robustness of our results against a different prior space. When sampling the likelihood distribution, we notice that the label switching issue between the (2, 2, 0) and (2, 2, 1) mode would sometimes occur, in which the sampler would explore where the A_{220} is almost zero, and A_{221} is favored associated with much heavier remnant mass. This is because the (2, 2, 1) mode of the template is locked on the (2, 2, 0) signal in the data.

In light of this issue, we choose to sample on the relative amplitude between the (2,2,1) mode and (2,2,0) mode, $A_{221}^{\text{rel}} = A_{221}/A_{220}$, instead of the absolute amplitude. We choose A_{221}^{rel} to be uniform in $[0, 5]$, and sample on $\log_{10} A_{220}$ which is uniformly distributed in $[-24, -19]$.

The results of Bayes factors are shown in Fig. 7. We only show the results from $f_s = 1024$ and 8192 Hz; other sampling rates present consistent conclusions. We note that the two parameterizations agree with each other well. At zero epoch, the relative amplitude parameterization slightly prefers a lower \mathcal{B}_{220}^{221} , which can be attributed to a slightly higher weight in the prior space for $A_{221} = 0$. At a sufficiently late time, the relative parameterization favors a Bayes factor being 1 between the (2, 2, 1) + (2, 2, 0) and (2, 2, 0) mode, i.e., no preference for any one of the models. Overall, the results demonstrate the robustness of the Bayes factor results in the main text.

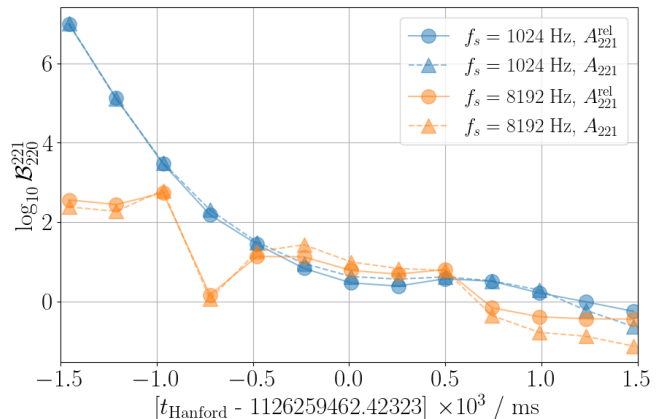


FIG. 7. Comparison of Bayes factor for a different parameterization that samples on A_{221}^{exc} and $\log_{10} A_{220}$.

Appendix C: Proof for the solution of inpainting

Recall that the Gaussian likelihood for the noise \mathbf{n} is

$$\log \mathcal{L} = -\frac{1}{2} \mathbf{n}^T C^{-1} \mathbf{n}. \quad (\text{C1})$$

As firstly introduced in [27], they construct an inpainting operator

$$F = 1 - AM^{-1}A^T C^{-1} \quad (\text{C2})$$

where $M = A^T C^{-1} A$. The matrix A is an “extraction matrix” with the size $N \times M$, where N and M are the numbers of elements of \mathbf{n} , and \mathbf{x} , the bad data to be inpainted, respectively. Explicitly, A is an identity matrix in the rows corresponding to \mathbf{x} and zeros elsewhere

$$A = \begin{pmatrix} 0 & & & & & \\ & 1 & \dots & & & \\ & & 1 & \dots & & \\ & & & 1 & \dots & \\ & & & & \dots & \dots & 1 \\ & & & & & & & 0 \end{pmatrix} \quad (\text{C3})$$

Such construction will have the desirable property that, after acting F on \mathbf{n} , any elements in the gating region will not impact the computation of $\mathbf{n}^T C^{-1} F \mathbf{n}$.

We offer another perspective, which is mathematically equivalent to [27], by considering the inverse of the covariance from the truncated data. Without loss of generality, we express $\mathbf{n}_{\text{inpaint}}$ as the concatenation of the truncated data and the (yet unknown) inpainting data, $\mathbf{n}_{\text{inpaint}} = \mathbf{n}_{\text{tr}} \oplus \mathbf{x}$ (the more general case that \mathbf{x} is in the middle of $\mathbf{n}_{\text{inpaint}}$ can be obtained by acting permutation matrix on it, and the following derivation remains the same). Hence the covariance matrix can be formally expressed by a block matrix, its inversion is

$$C^{-1} = \begin{pmatrix} C_{\text{tr}} & B \\ B^T & D \end{pmatrix}^{-1} = \begin{pmatrix} a & b \\ b^T & d \end{pmatrix} \quad (\text{C4})$$

where B, D, a, b, d are all block matrices yet unknown. Because of the inversion relation, we have

$$\begin{aligned} C_{\text{tr}} a + B b^T &= \mathbf{1} \\ C_{\text{tr}} b + B d &= \mathbf{0} \end{aligned} \quad (\text{C5})$$

where $\mathbf{1}$ and $\mathbf{0}$ are the unity and zero matrix, respectively. Express B by the second line of Eq. (C5) and insert to the first line, one gets

$$C_{\text{tr}}^{-1} = a - b d^{-1} b^T \quad (\text{C6})$$

Hence the likelihood of truncated data can be written as

$$\mathbf{n}_{\text{tr}}^T C_{\text{tr}}^{-1} \mathbf{n}_{\text{tr}} = \mathbf{n}_{\text{tr}}^T a \mathbf{n}_{\text{tr}} - \mathbf{n}_{\text{tr}}^T b d^{-1} b^T \mathbf{n}_{\text{tr}} \quad (\text{C7})$$

In the main text we have introduced the solution to be

$$C^{-1}(\mathbf{n}_{\text{tr}} \oplus \mathbf{x})_{\text{inpaint}} = \mathbf{0}_{\text{inpaint}} \quad (\text{C8})$$

This can be expressed as

$$b^T \mathbf{n}_{\text{tr}} + d \mathbf{x} = \mathbf{0} \quad (\text{C9})$$

Hence

$$\mathbf{x} = -d^{-1} b^T \mathbf{n}_{\text{tr}} \quad (\text{C10})$$

Therefore

$$\begin{aligned} &(\mathbf{n}_{\text{tr}} \oplus \mathbf{x})^T C^{-1}(\mathbf{n}_{\text{tr}} \oplus \mathbf{x}) \quad (\text{C11}) \\ &= (\mathbf{n}_{\text{tr}} \oplus \mathbf{x})^T \begin{pmatrix} a & b \\ b^T & d \end{pmatrix} (\mathbf{n}_{\text{tr}} \oplus \mathbf{x}) \\ &= \mathbf{n}_{\text{tr}}^T a \mathbf{n}_{\text{tr}} - \mathbf{n}_{\text{tr}}^T b d^{-1} b^T \mathbf{n}_{\text{tr}} \end{aligned}$$

Together with Eq. (C7) we have proved that inpainting with \mathbf{x} will resume the use of C^{-1} in the likelihood. As discussed in [26], constructing the inpainting filter directly as in Eq. (C2) invokes inverting the $A^T C^{-1} A$ which requires M^3 time complexity. However, as we use Levinson Recursion in `scipy` [43] to solve the Toeplitz linear equation for inpainting data in Eq. (C8), it only requires the M^2 time complexity.

-
- [1] Roberto Cotesta, Gregorio Carullo, Emanuele Berti, and Vitor Cardoso, “Analysis of Ringdown Overtones in GW150914,” *Phys. Rev. Lett.* **129**, 111102 (2022), [arXiv:2201.00822 \[gr-qc\]](#).
- [2] Maximiliano Isi, Matthew Giesler, Will M. Farr, Mark A. Scheel, and Saul A. Teukolsky, “Testing the no-hair theorem with GW150914,” *Phys. Rev. Lett.* **123**, 111102 (2019), [arXiv:1905.00869 \[gr-qc\]](#).
- [3] Maximiliano Isi and Will M. Farr, “Revisiting the ringdown of GW150914,” (2022), [arXiv:2202.02941 \[gr-qc\]](#).
- [4] C. V. Vishveshwara, “Scattering of gravitational radiation by a schwarzschild black-hole,” *Nature* **227**, 936–938 (1970).
- [5] Werner Israel, “Event horizons in static vacuum spacetimes,” *Phys. Rev.* **164**, 1776–1779 (1967).
- [6] B. Carter, “Axisymmetric black hole has only two degrees of freedom,” *Phys. Rev. Lett.* **26**, 331–333 (1971).
- [7] Olaf Dreyer, Bernard J. Kelly, Badri Krishnan, Lee Samuel Finn, David Garrison, and Ramon Lopez-Aleman, “Black hole spectroscopy: Testing general relativity through gravitational wave observations,” *Class. Quant. Grav.* **21**, 787–804 (2004), [arXiv:gr-qc/0309007](#).
- [8] B. P. Abbott *et al.* (LIGO Scientific, Virgo), “Tests of general relativity with GW150914,” *Phys. Rev. Lett.* **116**, 221101 (2016), [Erratum: *Phys.Rev.Lett.* 121, 129902 (2018)], [arXiv:1602.03841 \[gr-qc\]](#).
- [9] Miriam Cabero, Julian Westerweck, Collin D. Capano, Sumit Kumar, Alex B. Nielsen, and Badri Krishnan, “Black hole spectroscopy in the next decade,” *Phys. Rev. D* **101**, 064044 (2020), [arXiv:1911.01361 \[gr-qc\]](#).
- [10] J. Aasi *et al.* (LIGO Scientific), “Advanced LIGO,” *Class. Quant. Grav.* **32**, 074001 (2015), [arXiv:1411.4547 \[gr-qc\]](#).
- [11] F. Acernese *et al.* (VIRGO), “Advanced Virgo: a second-generation interferometric gravitational wave detector,” *Class. Quant. Grav.* **32**, 024001 (2015), [arXiv:1408.3978 \[gr-qc\]](#).
- [12] Homare Abe *et al.* (KAGRA), “The current status and future prospects of kagra, the large-scale cryogenic gravitational wave telescope built in the kamioka underground,” *Galaxies* **10** (2022), [10.3390/galaxies10030063](#).
- [13] R. Abbott *et al.* (LIGO Scientific, Virgo), “GW190521: A Binary Black Hole Merger with a Total Mass of 150 M_{\odot} ,” *Phys. Rev. Lett.* **125**, 101102 (2020), [arXiv:2009.01075 \[gr-qc\]](#).
- [14] R. Abbott *et al.* (LIGO Scientific, Virgo), “Properties and Astrophysical Implications of the 150 M_{\odot} Binary Black Hole Merger GW190521,” *Astrophys. J. Lett.* **900**, L13 (2020), [arXiv:2009.01190 \[astro-ph.HE\]](#).
- [15] Collin D. Capano, Miriam Cabero, Julian Westerweck, Jahed Abedi, Shilpa Kastha, Alexander H. Nitz, Yi-Fan Wang, Alex B. Nielsen, and Badri Krishnan, “Observation of a multimode quasi-normal spectrum from a per-

- turbed black hole,” (2021), [arXiv:2105.05238 \[gr-qc\]](#).
- [16] Collin D. Capano, Jahed Abedi, Shilpa Kastha, Alexander H. Nitz, Julian Westerweck, Yi-Fan Wang, Miriam Cabero, Alex B. Nielsen, and Badri Krishnan, “Statistical validation of the detection of a sub-dominant quasinormal mode in GW190521,” (2022), [arXiv:2209.00640 \[gr-qc\]](#).
- [17] Xisco Jiménez Forteza, Swetha Bhagwat, Sumit Kumar, and Paolo Pani, “Novel Ringdown Amplitude-Phase Consistency Test,” *Phys. Rev. Lett.* **130**, 021001 (2023), [arXiv:2205.14910 \[gr-qc\]](#).
- [18] Jahed Abedi, Collin D. Capano, Shilpa Kastha, Yi-Fan Wang, Julian Westerweck, Alex B. Nielsen, and Badri Krishnan, “Spectroscopy for asymmetric binary black hole mergers,” (2023), [arXiv:2309.03121 \[gr-qc\]](#).
- [19] Harrison Siegel, Maximiliano Isi, and Will Farr, “The Ringdown of GW190521: Hints of Multiple Quasinormal Modes with a Precessional Interpretation,” (2023), [arXiv:2307.11975 \[gr-qc\]](#).
- [20] Matthew Giesler, Maximiliano Isi, Mark A. Scheel, and Saul Teukolsky, “Black Hole Ringdown: The Importance of Overtones,” *Phys. Rev. X* **9**, 041060 (2019), [arXiv:1903.08284 \[gr-qc\]](#).
- [21] Juan Calderón Bustillo, Paul D. Lasky, and Eric Thrane, “Black-hole spectroscopy, the no-hair theorem, and GW150914: Kerr versus Occam,” *Phys. Rev. D* **103**, 024041 (2021), [arXiv:2010.01857 \[gr-qc\]](#).
- [22] Eliot Finch and Christopher J. Moore, “Searching for a ringdown overtone in GW150914,” *Phys. Rev. D* **106**, 043005 (2022), [arXiv:2205.07809 \[gr-qc\]](#).
- [23] Sizheng Ma, Ling Sun, and Yanbei Chen, “Using rational filters to uncover the first ringdown overtone in GW150914,” *Phys. Rev. D* **107**, 084010 (2023), [arXiv:2301.06639 \[gr-qc\]](#).
- [24] Marco Crisostomi, Kallol Dey, Enrico Barausse, and Roberto Trotta, “Neural posterior estimation with guaranteed exact coverage: The ringdown of GW150914,” *Phys. Rev. D* **108**, 044029 (2023), [arXiv:2305.18528 \[gr-qc\]](#).
- [25] Gregorio Carullo, Walter Del Pozzo, and John Veitch, “Observational Black Hole Spectroscopy: A time-domain multimode analysis of GW150914,” *Phys. Rev. D* **99**, 123029 (2019), [Erratum: *Phys.Rev.D* 100, 089903 (2019)], [arXiv:1902.07527 \[gr-qc\]](#).
- [26] Maximiliano Isi and Will M. Farr, “Analyzing black-hole ringdowns,” (2021), [arXiv:2107.05609 \[gr-qc\]](#).
- [27] Barak Zackay, Tejaswi Venumadhav, Javier Roulet, Liang Dai, and Matias Zaldarriaga, “Detecting gravitational waves in data with non-stationary and non-Gaussian noise,” *Phys. Rev. D* **104**, 063034 (2021), [arXiv:1908.05644 \[astro-ph.IM\]](#).
- [28] C. M. Biwer, Collin D. Capano, Soumi De, Miriam Cabero, Duncan A. Brown, Alexander H. Nitz, and V. Raymond, “PyCBC inference: A python-based parameter estimation toolkit for compact binary coalescence signals,” *Publications of the Astronomical Society of the Pacific* **131**, 024503 (2019).
- [29] Bruce Allen, Warren G. Anderson, Patrick R. Brady, Duncan A. Brown, and Jolien D. E. Creighton, “FIND-CHIRP: An Algorithm for detection of gravitational waves from inspiraling compact binaries,” *Phys. Rev. D* **85**, 122006 (2012), [arXiv:0509116 \[gr-qc\]](#).
- [30] Joshua S Speagle, “dynesty: a dynamic nested sampling package for estimating Bayesian posteriors and evidences,” *Monthly Notices of the Royal Astronomical Society* **493**, 3132–3158 (2020), <https://academic.oup.com/mnras/article-pdf/493/3/3132/32890730/staa278.pdf>.
- [31] Alexander H. Nitz, Collin D. Capano, Sumit Kumar, Yi-Fan Wang, Shilpa Kastha, Marlin Schäfer, Rahul Dhurkunde, and Miriam Cabero, “3-OGC: Catalog of Gravitational Waves from Compact-binary Mergers,” *Astrophys. J.* **922**, 76 (2021), [arXiv:2105.09151 \[astro-ph.HE\]](#).
- [32] Alexander H. Nitz, Sumit Kumar, Yi-Fan Wang, Shilpa Kastha, Shichao Wu, Marlin Schäfer, Rahul Dhurkunde, and Collin D. Capano, “4-OGC: Catalog of Gravitational Waves from Compact Binary Mergers,” *Astrophys. J.* **946**, 59 (2023), [arXiv:2112.06878 \[astro-ph.HE\]](#).
- [33] Collin D. Capano, “In preparation,” (2023).
- [34] Benjamin P Abbott *et al.* (LIGO Scientific, Virgo), “A guide to LIGO–Virgo detector noise and extraction of transient gravitational-wave signals,” *Class. Quant. Grav.* **37**, 055002 (2020), [arXiv:1908.11170 \[gr-qc\]](#).
- [35] Benjamin P. Abbott *et al.* (LIGO Scientific, Virgo), “The basic physics of the binary black hole merger GW150914,” *Annalen Phys.* **529**, 1600209 (2017), [arXiv:1608.01940 \[gr-qc\]](#).
- [36] Gregorio Carullo, Gunnar Riemenschneider, Ka Wa Tsang, Alessandro Nagar, and Walter Del Pozzo, “GW150914 peak frequency: a novel consistency test of strong-field General Relativity,” *Class. Quant. Grav.* **36**, 105009 (2019), [arXiv:1811.08744 \[gr-qc\]](#).
- [37] Bruce Allen, “ χ^2 time-frequency discriminator for gravitational wave detection,” *Phys. Rev. D* **71**, 062001 (2005), [arXiv:gr-qc/0405045](#).
- [38] Vishal Baibhav, Mark Ho-Yeuk Cheung, Emanuele Berti, Vitor Cardoso, Gregorio Carullo, Roberto Cotesta, Walter Del Pozzo, and Francisco Duque, “Agnostic black hole spectroscopy: quasinormal mode content of numerical relativity waveforms and limits of validity of linear perturbation theory,” (2023), [arXiv:2302.03050 \[gr-qc\]](#).
- [39] Peter James Nee, Sebastian H. Völkel, and Harald P. Pfeiffer, “Role of black hole quasinormal mode overtones for ringdown analysis,” *Phys. Rev. D* **108**, 044032 (2023), [arXiv:2302.06634 \[gr-qc\]](#).
- [40] M. Isi and W. M. Farr, “Comment on ‘analysis of ringdown overtones in gw150914’,” *Phys. Rev. Lett.* **131**, 169001 (2023).
- [41] Gregorio Carullo, Roberto Cotesta, Emanuele Berti, and Vitor Cardoso, “Carullo et al. reply:,” *Phys. Rev. Lett.* **131**, 169002 (2023).
- [42] “Data release associated with ‘A frequency-domain perspective on GW150914 ringdown overtone’,” <https://github.com/gwastro/gw150914-overtone>.
- [43] Pauli Virtanen *et al.*, “SciPy 1.0—Fundamental Algorithms for Scientific Computing in Python,” *Nature Meth.* **17**, 261 (2020), [arXiv:1907.10121 \[cs.MS\]](#).